The use of neutron inelastic scattering and hydrogen isotope exchange to investigate the nature of sites occupied by hydrogen in $TiMn_{1.5}$

1989 J. Phys.: Condens. Matter 1 6025

(http://iopscience.iop.org/0953-8984/1/35/003)

J. Phys.: Condens. Matter **1** (1989) 6025–6037. Printed in the UK

The use of neutron inelastic scattering and hydrogen isotope exchange to investigate the nature of sites occupied by hydrogen in $TiMn_{1.5}$

P W Albers†, G H Sicking‡ and D K Ross§

† Degussa AG, Zweigniederlassung Wolfgang, Postfach 13 45, 6450 Hanau 1, Federal Republic of Germany

‡ Verbundzentrum für Oberflächen- und Mikrobereichsanalyse (VOM), Universität Münster, Wilhelm-Klemm-Strasse 10, 4400 Münster, Federal Republic of Germany

§ School of Physics and Space Research, University of Birmingham, PO Box 363, Birmingham B15 2TT, UK

Received 10 January 1989

Abstract. Inelastic neutron scattering and isotope separation factor measurements are reported for the potential hydrogen storage system $Ti_{0.4}Mn_{0.6}H_n$. Inelastic spectra were measured for six hydrogen concentrations ranging from 0.001 to 1.0 hydrogens/metal atom, the first five in the α and $\alpha + \beta$ phases and the last in the β phase. The spectra consisted of two groups of peaks, the first from 70 meV to 110 meV and the second from 110 to 180 meV. The intensity of the former was independent of the hydrogen content and could be associated with a precursor region in the isotherm while that of the latter rose linearly with hydrogen content. Peak shape analysis of the high energy peaks show them to be consistent with occupation of first Ti_3Mn and then Ti_2Mn_2 sites and with changes between the α- and β-phases. The identification of the precursor sites is not easy if based entirely on the IINS spectra as both –OH and near surface interstitial sites could be involved. However, the measurement of the H/T isotope separation factor unambiguously points to the existence of TiOH because only this can explain the dramatic fall of α near $n = 0$.

1. Introduction

Inelastic incoherent neutron scattering (IINS) on metal/hydrogen systems is able to reveal the dynamics of interstitial hydrogen [1]. The most important frequency range is 10^{12}–$10^{14}\ s^{-1}$ (4–400 meV). The hydrogen undergoes jump diffusion through the lattice with a mean jump rate of up to $10^{12}\ s^{-1}$ (~4 meV), the acoustic phonons extend up to $10^{13}\ s^{-1}$ (40 meV) and the optical phonons and local modes are found in the range 1.5×10^{13} to $10^{14}\ s^{-1}$ (60–400 meV). Due to the very favourable cross sections of H for inelastic neutron scattering, IINS is able to determine the amplitude-weighted phonon-density of states of the hydrogen down to very low concentrations. The vibration frequencies of the hydrogen atoms can give valuable informations on the metal/hydrogen interaction and on the symmetry of the interstitial sites occupied by the hydrogen atoms.

The low-energy vibrations of hydrogen are closely related to the acoustic phonons of the host-lattice: these vibrations can be found at energies of <30 meV and are called

0953-8984/89/356025 + 13 $02.50

band modes. When the hydrogen vibrations are in antiphase with those of the lattice, the frequencies are much higher (60–400 meV). At high (stoichiometric) concentrations, these frequencies may be determined from the optical dispersion curves. At lower concentrations, the protons vibrate independently of each other and can be described as isolated Einstein oscillators.

For the case of alloy systems and intermetallic compounds [2], the interstitial sites are formed from different geometric configurations of the host lattice atoms. For instance for tetrahedral sites in AB_2 compounds, independent variations of the hydrogen occupation on different types of site are possible. The energies of these modes and their degeneracy can give information about the local symmetry of the interstitial sites occupied, as a function of increasing hydrogen concentration. The frequencies of protons on octahedral sites are typically around 60 meV, while for tetrahedral sites values around 150 meV were usually found [3–5].

In the present paper, we report the use of IINS for observing the changes of site occupation for the system $Ti_{0.4}Mn_{0.6}H_n$ (sometimes written $TiMn_{1.5}H_x$) as a function of the hydrogen concentration n. Our interest was focused on this system because it has a convenient plateau pressure of about 7 bar at room temperature and is therefore of technical importance for storing hydrogen isotopes. The frequencies of vibrations of hydrogen isotopes in interstitial sites are the most important quantities by which the hydrogen isotope equilibrium distribution between gas phase and solid phase is determined [6]. Thus, measurement of the so-called isotope separation factor, α, is a valuable and independent method for determining local mode frequencies. IINS- and α-measurements supplement each other and a comparison of both can give additional information about the state of hydrogen within the metal, as will be shown in the present paper.

2. Characteristics of AB_2- and $AB_{1.5}$-compounds

Intermetallic compounds of the C14 and C15 structure are well known for their excellent hydrogen absorption properties. The AB_2 compounds, and the off-stoichiometric variants, $AB_{1.5}$, of the elements A = Ti, Zr, and B = Mn have been the subjects of a number of investigations using various experimental methods. Beside their suitability for large scale technical application as hydrogen storage materials [7, 8] and for hydrogen isotope separation [9, 10], the special surface conditions and the structural changes to the surface due to hydrogen cycling [8–14] have been investigated.

The surfaces of the $AB_{1.5}$ materials are modified by hydrogen absorption: the hydrogen-induced segregation of oxygen impurities and of the strong hydride forming component Ti(Zr) to the solid surface, accompanied by hydrogen embrittlement leads to an active coating of the material, containing Ti- or Zr-hydride [10, 13]. Additional structural changes have been presented in a paper [14] dealing with the influence of non-stoichiometry (deviation from the pure AB_2 composition). These non-stoichiometric compounds also have rather different bulk behaviour. Thus Didisheim *et al* [15] have shown, using neutron diffraction on $ZrMn_2D_3$, that the hydrogen isotope is located on interstitial sites formed by Zr_2Mn_2 and $ZrMn_3$ tetrahedra. Changing the AB_2- to the $AB_{1.5}$-composition will in principle give new kinds of interstitial sites with different occupancy factors. The tetrahedral sites with the higher hydrogen affinity should be filled preferentially. This was shown by Fruchart and co-workers [16]: neutron diffraction measurements on $TiMn_{1.5}H_{2.5}$ yielded the fact that, in this non-stoichiometric hexagonal C14 Laves phase, the 'excess Ti' introduced into the manganese sublattice is only located

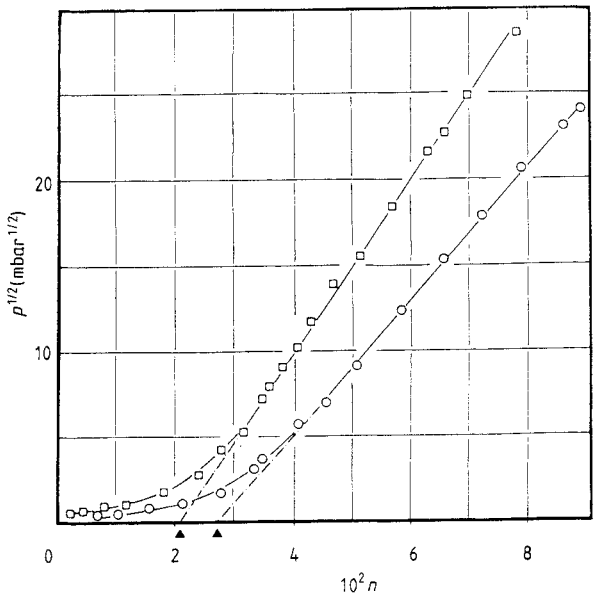

Figure 1. Hydrogen sorption isotherms of $Ti_{0.4}Mn_{0.6}$ at 273 K (circles) and 303 K (squares). The extrapolated precursor regions are indicated by full triangles.

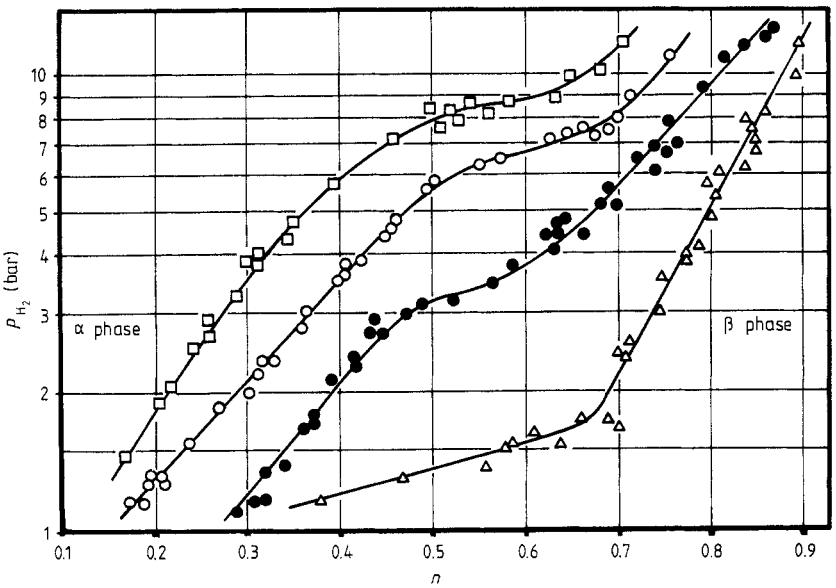

Figure 2. Hydrogen absorption isotherms of $Ti_{0.4}Mn_{0.6}$ at 253 K (triangles), 273 K (full circles), 293 K (open circles) and 313 K (squares).

on 2*a*-sites, forming a new kind of interstitial site, the tetrahedral Ti_3Mn site, which does not exist in the $TiMn_2$ (AB_2) compound. Hydrogen does not enter the $TiMn_3$ or the Mn_4 sites, only the Ti_2Mn_2 and the Ti_3Mn sites.

Figures 1 and 2 show some hydrogen sorption isotherms for $Ti_{0.4}Mn_{0.6}$. At low pressures, a precursor region (figure 1) has been found [10] before the onset of the usual $\sqrt{p}$ 'Sieverts-behaviour' range, which is typical of dissociative hydrogen absorption.

This precursor region is due to hydrogen absorption in surface or subsurface states, as surface hydride layers are formed. It is known [10] that hydrogen absorption produces distinct O- and Ti-segregation at the solid surface, hence producing a very active Ti-hydride coating, which is assumed to be responsible for the excellent hydriding/dehydriding kinetics of this material. The same behaviour was found for the related $ZrMn_x$ systems. In this context, the role of the oxygen that segregates to the surface simultaneously with Ti(Zr), is not known, so far. There has been some speculation about the formation of OH-groups and the present paper will clarify this question.

Figure 2 shows the sorption characteristics of $TiMn_{1.5}$ over the whole range (α-phase/two-phase region/β-phase). The n values (the hydrogen/metal atom ratio), quoted for the various neutron spectra from $Ti_{0.4}Mn_{0.6}H_n$, refer to these isotherms.

3. Experimental details

The preparation, homogenisation and physical and metallurgical characterisation of the $TiMn_{1.5}$ Laves-phase compound (the starting material) were described in detail elsewhere [14].

The IINS measurements were carried out utilising the following research facilities: the Be-filter triple axis spectrometer (BFTAS) at the DIDO reactor AERE, Harwell (UK); and the IN1B spectrometer at the ILL, Grenoble (France). The spectra were all recorded at a sample temperature of 77 K. For neutron scattering experiments on hydride systems, it is best to use samples with a total plane density of around 2×10^{21} protons cm^{-2}. Using a cross section of 80 barns ($1\ b = 10^{-28}\ m^2$), this corresponds to 16% scattering in a sample normal to the beam. Multiple scattering events are not too severe in these conditions. Thus, the highly concentrated β-phase samples were about 0.5–1.0 mm thick but for the very diluted α-phase samples 1–2 cm of path length were required. If the effective neutron beam area is about 16 cm^2, samples in the 100 g scale have to be prepared. The preparation involves in-situ hydrogen cycling and hence activation. Volumetric determination of the adjusted hydrogen concentration is essential to avoid uncertainties due to unknown amounts of unspecified surface hydrogen states in the α-phase materials, especially those introduced during the handling of the (occasionally pyrophoric) hydrides under inert gas atmospheres or in air. Aluminium and stainless steel (1.4301, ANSI 304) vessels were constructed for reacting the intermetallic compounds with hydrogen (purity 99.999%), for cycling through the phase diagram, and for adjusting the appropriate hydrogen concentration for a particular neutron experiment. Thus the whole procedure, starting with the compact alloy material (ingots) and ending with a finely divided hydride powder with a surface area of some m^2/g took place inside the sample chamber. The hydrogen loading was performed using a new high vacuum/high pressure rig. The amount of hydrogen dissolved in the specimens after cycling, was determined by gas volumetric methods, using mechanical precision gauges and MKS-Baratron capacitance gauges. Each sample was hydrided/dehydrided at least 7 times. Before the final hydrogenation, the sample cans were heated up to 450 °C under high vacuum conditions to thoroughly degas the sample and the calculated volume of hydrogen was then added. It should be noted that this process establishes the total reversible hydrogen content of each sample but that any irreversibly bound hydrogen introduced in the earlier cycles will be in addition to this concentration. After equilibrium was established between hydrogen and the solid hydride phase at a controlled temperature, the sample vessels were sealed and inserted into the cryostats of the particular

neutron facility. For the case of $Ti_{0.4}Mn_{0.6}H_n$, we have investigated the whole concentration range, starting with the very dilute α-phase, through the two phase region and up to near the stoichiometric β-hydride phase concentration. The measurements of the equilibrium separation factor for the α-phase of $Ti_{0.4}Mn_{0.6}H_n$, α, for equilibrium pressures up to one bar hydrogen were described earlier [10]. Briefly the principles of separation factor measurements with tritium as a tracer isotope are as follows:

(i) The intermetallic compound is first equilibrated with pure protium at given values of p and T (sorption equilibrium).

(ii) Part of the gas phase is substituted by a tracer mixture of tritium and protium.

(iii) The metal-hydride is allowed to exchange protium for tritium from the gas phase until equilibrium is established (isotope exchange equilibrium).

(iv) The isotope equilibrium is determined from the decrease of the tritium content in the gas phase, measured by means of an ionisation chamber.

We have since extended the separation factor measurements to higher pressures of about 11 bar at 273 K. For this purpose a stainless steel loop reactor was constructed, similar to the earlier version that was made from glass components [10]. By inspection of figure 2 it is evident that the separation factors measured cover the region from dilute α-phase ($n = 0.02$) up to pure β-phase ($n = 0.83$) and cross the two-phase region (all measurements at 273 K). Thus the IINS-measurements and the separation factor measurements relate to the same concentration range and may be directly compared.

4. Results

Figures 3(*a*) to 3(*f*) show spectra of $Ti_{0.4}Mn_{0.6}H_n$-samples with increasing hydrogen content n, starting with $n = 0.001$ and ending up at $n = 1.001$. The spectra are presented on an energy transfer scale, obtained from the incident energy by subtracting the mean transmission energy for the particular beryllium filter, and have been corrected for background (spline fitted for samples 3*b* to 3*f*). The total peak areas were in the range from 8000 to 12000 counts except for 3*f*, which was about 19000 counts.

The shape of the isotherms would suggest the existence of an $\alpha + \beta$ phase region which at 253 K extends from roughly $n = 0.35$ to $n = 0.67$. A sloping plateau is to be expected because of the presence of titanium in the manganese sublattice. At 80 K, the maximum concentration in solid solution will probably be lower still, depending on how a particular sample was cooled. Thus spectrum 3(*a*) refers to the 'pre-Sieverts' precursor region while 3(*b*), although apparently in the 'pre-Sieverts' region certainly shows evidence of a new type of site. Spectra 3(*c*), 3(*d*) and 3(*e*) are probably in the two phase region and spectrum 3(*f*) is well into the β-phase.

The spectra show basically two groups of peaks, a low energy peak at about 74 meV which, at all but the lowest concentration, spreads towards higher energies, and a higher energy group in the 110 to 180 region. The spectra were fitted to Gaussian profiles using three peaks in each region (one in each for the case of 3(*a*)). The fits are good in the high energy region but must be treated with some caution in the low energy group.

The peak energies are given in table 1. It should be emphasised that, while the 74 meV peak is well determined, the other two peaks in the low energy group, although necessary to match the spectral shape, are not well determined in the fitting process. The integrated intensities of the lower, Γ_{Lo}, and higher, Γ_{Hi}, energy groups, along with

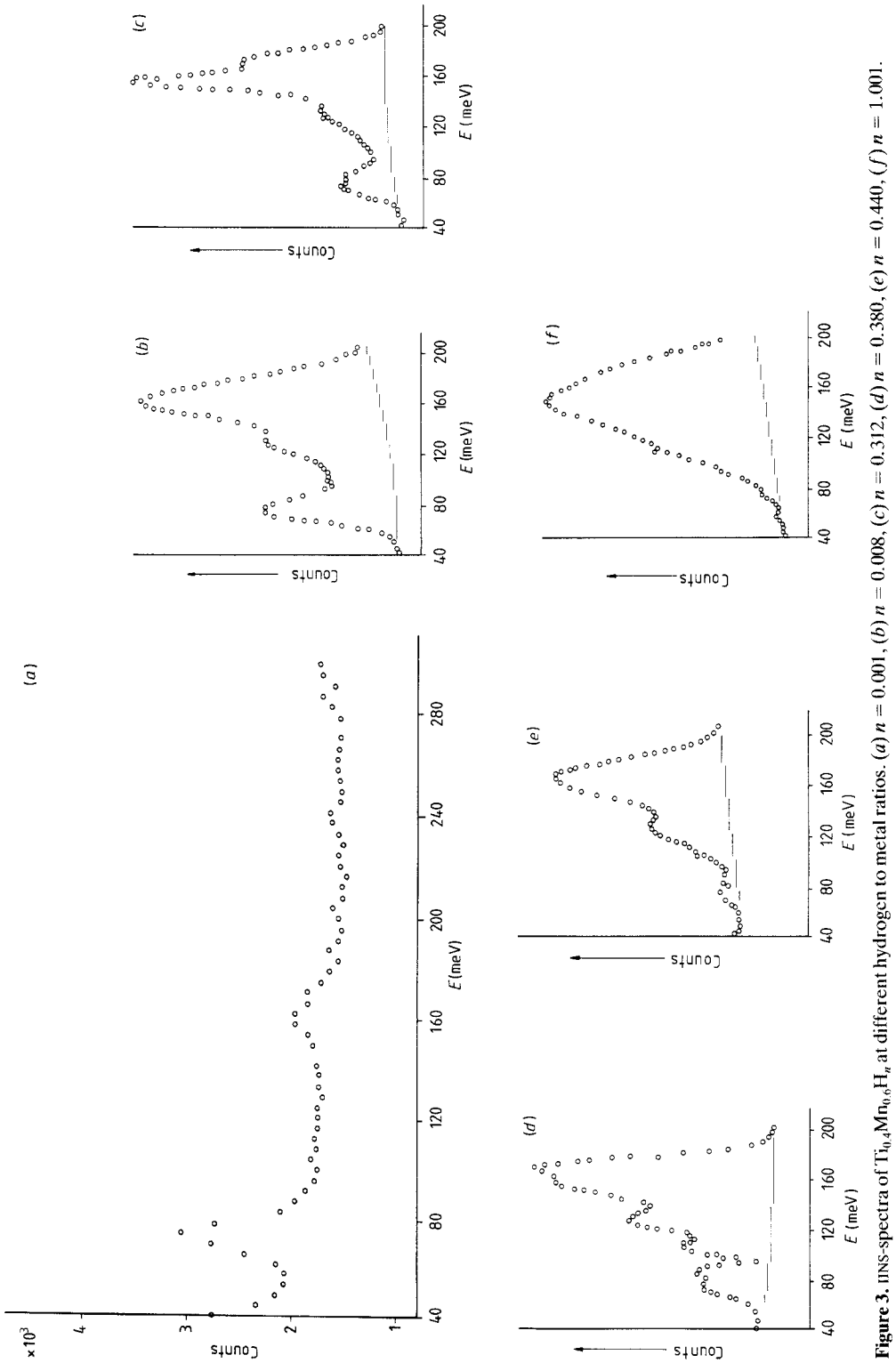

Figure 3. INS-spectra of $Ti_{0.4}Mn_{0.6}H_n$ at different hydrogen to metal ratios. (*a*) $n = 0.001$, (*b*) $n = 0.008$, (*c*) $n = 0.312$, (*d*) $n = 0.380$, (*e*) $n = 0.440$, (*f*) $n = 1.001$.

Table 1. Peak energies obtained by fitting six Gaussians to the spectra in figure 3, with the corresponding H/M ratio, n.

		Low energy group			High energy group		
Figure No	n	Peak 1 [meV]	Peak 2 [meV]	Peak 3 [meV]	Peak 4 [meV]	Peak 5 [meV]	Peak 6 [meV]
3*a*	0.001	74.0	—	—	—	160.0	—
3*b*	0.008	73.6	83.7	100.3	133.2	162.5	177.8
3*c*	0.312	74.4	85.8	94.9	139.9	160.0	177.7
3*d*	0.380	75.3	89.0	107.0	130.3	156.5	173.7
3*e*	0.440	76.2	88.3	108.1	130.0	161.9	178.5
3*f*	1.001	75.1	75.2	90.8	116.7	145.8	172.7

Table 2. Values of the fitted areas for the low and high energy groups of peaks, with n values, sample weights and equilibrium hydrogen pressures at 273 K.

Figure No	n	Γ_{LO}	Γ_{Hi}	Weight [g]	p [bar]
3*a*	0.001	0.653	0.347	62.5	<0.002
3*b*	0.008	0.259	0.741	107.0	0.448
3*c*	0.312	0.139	0.861	20.8	1.220
3*d*	0.380	0.177	0.823	7.8	1.981
3*e*	0.440	0.029	0.971	3.6	2.890
3*f*	1.001	0.002	0.998	2.5	28.0

the weight of the samples and the equilibrium hydrogen pressures at 273 K are given in table 2.

Table 3 gives the measured α-values and the equilibrium pressures, together with the corresponding n-values. The numbers in brackets indicate the number of independent measurements that were averaged to give the corresponding α-value.

The separation factor α is related to the equilibrium (tracer) distribution of the tritium isotope between hydrogen in the gas phase (G) and hydrogen in the solid phase (S) and is defined as

$$\alpha = x^{G}/x^{S} \tag{1}$$

with x the atomic fraction of tritium in the corresponding phase. Within the pressure region investigated, the α-values are always smaller than unity, implying that the heavy hydrogen isotope is enriched in the solid phase. This enrichment increases sharply at low equilibrium pressures, where α-values of about 0.3 are found. At medium and high equilibrium pressures the α-values are around 0.74 and 0.82, respectively, indicating a moderate isotope enrichment.

Referring to figures 1 and 2 the α-values No 1–5 related to the precursor region, No 6–18 to the α-phase, No 19–22 to the α/β-two-phase region and No 23–29 to the β-phase.

5. Discussion

The lowest concentration sample (spectrum 3(*a*)) is clearly in the precursor region, and the strong peak at 74 meV can be attributed to a strongly bound surface site. This peak

Table 3. Values of the equilibrium pressures, p, and the isotopic separation factor, α, at a series of H/M ratios, n, measured at 273 K.

No	α	p [mbar]	n
1	0.332	2.7	0.0201
2	0.462	2.7	0.0201
3	0.405	8.7	0.0222
4	0.438 (2)	10.7	0.0252
5	0.566	16.7	0.0278
6	0.548	31.2	0.0302
7	0.553 (2)	34.0	0.0318
8	0.656	48.0	0.0325
9	0.643	69.2	0.0369
10	0.668 (2)	84.0	0.0392
11	0.741 (4)	136.0	0.0458
12	0.639 (2)	153.2	0.0479
13	0.745 (3)	273.2	0.0705
14	0.681 (2)	332.0	0.0772
15	0.762 (2)	1148	0.285
16	0.755 (2)	1289	0.315
17	0.749 (2)	1638	0.365
18	0.747 (2)	1767	0.372
19	0.772 (2)	2888	0.479
20	0.778 (2)	3107	0.520
21	0.821	3525	0.565
22	0.763 (2)	4323	0.620
23	0.811 (2)	4416	0.635
24	0.823 (2)	4686	0.660
25	0.801	5634	0.685
26	0.810 (2)	6796	0.735
27	0.807 (2)	7743	0.743
28	0.811	8972	0.795
29	0.832	11 021	0.826

appears in the subsequent spectra (3(*b*)–3(*e*)) with decreasing relative intensity and has essentially disappeared in figure 3(*f*). In figure 4 we show plots of $n\Gamma_{Lo}$ and $n\Gamma_{Hi}$, taken from table 2, plotted against n. The quantity $n\Gamma_{Lo}$ is the number of hydrogens/metal atom contributing to the low energy peak (peaks 1–3). The graph confirms that the site giving rise to this feature must already be fully saturated at low concentrations. The first harmonic of this peak must contribute to the weak feature at 160 meV in figure 3(*a*). The fitted area of this peak is about half of that of the fundamental, whereas harmonic theory would suggest that, for Be Filter spectrometers, it should be about $\frac{1}{3}$ of the intensity so that it may also contain some contribution from a higher energy fundamental mode. However, it is clear that this harmonic contribution will make a negligible contribution to the intensity in this region in the higher concentration samples.

At $n = 0.008$ (figure 3(*b*)), there is clearly a major new contribution in the higher energy region due to some different type of site. If the sample were clearly in the solid solution range, one would naturally associate it with a bulk site but because it seems to be in the precursor range, a new type of near-surface site may be involved. The possibilities are therefore:

(i) chemisorbed hydrogen

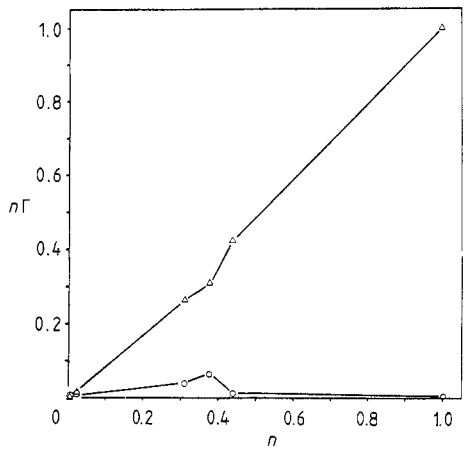

Figure 4. Plots of nΓ versus n for hydrogen vibrating in the low-energy region (circles) and hydrogen vibrating in the high-energy region (triangles).

(ii) hydrogen in segregated surface layers
(iii) hydrogen in sub-surface states
(iv) hydrogen in true bulk states

The main vibration energies, 133 and 162 meV, are compatible with any of these four explanations. Thus:

(i) from electron energy loss spectroscopy (HREELS), hydrogen chemisorbed in 'on-top' position on W(100) planes has a frequency corresponding to 155 meV [17];

(ii) As shown by Auger electron spectroscopy, [10, 18], in-situ high voltage electron microscopy [14] and elastic recoil detection [13] on the $Ti_{0.4}Mn_{0.6}$-($Zr_{0.4}Mn_{0.6}$-) systems, a hydrogen-induced Ti (Zr)-hydride is formed in the near-surface regions. The corresponding optical vibration frequency at 149 meV in TiH_2 [4] (141 meV for ZrH_2 [19]) indicates that the present peaks could be due to hydrogen in tetrahedral sites of near cubic symmetry in segregated Ti regions;

(iii) and (iv) sub-surface states and bulk states in the solid solution region will, of course, show IINS peaks close to the energies observed in the α and β phases (156–162 meV, 3(*c*)–3(*e*) and 146 meV, 3(*f*)).

For the next two concentrations ($n = 0.312$, figure 3(*c*); $n = 0.380$, figure 3(*d*)), the peak shapes are somewhat more complicated. One could relate this complexity to the two-phase region of the phase diagram, i.e. to tetrahedral sites in the α- and β-phase respectively, although, as mentioned above, it is difficult to be sure of the positions of the phase boundaries in such systems at 80 K. It will be seen that the highest energy component, at about 175 meV, is missing in figure 3(*b*), increases in figures 3(*c*) and 3(*d*) and completely dominates in figure 3(*e*) while the 160 meV component behaves in a converse way, thus suggesting that, at $n = 0.440$, the system is essentially in the β phase. However, this explanation is complicated by the existence of two types of tetrahedral sites in this system. The off-stoichiometric $TiMn_{1.5}$ compound is closely related to $TiMn_2$ Laves phase structure, where the excess Ti occupies the 2*a* site of the Mn-sublattice. Thus, Ti_3Mn sites are formed in addition to the normal Ti_2Mn_2 sites [16]. Due to the strong interaction between H and Ti, one expects that the Ti_3Mn sites (point-symmetry, C_{3v}) will be filled in preference to the Ti_2Mn_2 sites (point-symmetry, C_{2v}). The doublet in the high energy group in figure 3(*b*) is clearly consistent with C_{3v} symmetry and the more complex spectra of figures 3(*c*) and 3(*d*) could clearly include a triplet contribution.

Table 4. Energies of the characteristic vibrations of finely divided $Ni(OH)_2$ as measured by IINS [24] and the characteristic frequencies of the –OH vibrations.

A	ν(M–OH)	57 meV
B	δ(O–M–OH)	88 meV
C	ν(O–H)	400 meV
D	δ(O–H)	111.5 meV

However, in view of the fact that one might expect to find more of the C_{2v} sites occupied in the β-phase as compared to the α-phase, it is impossible to distinguish between these two explanations on the present evidence. Finally, in spectrum 3(f), the higher energy group completely dominates the spectrum and has become considerably broadened, probably due to H–H interactions and/or increased occupation of Ti_2Mn_2 sites at high concentrations. It is also noticeable that the middle peak energy has shifted down to 145 meV and this could be associated with the overall lattice expansion of 27.1% [20].

The strongest peak of the low energy group is at about 75 meV, a surprisingly low frequency, which cannot be explained by local modes of hydrogen in tetrahedral holes. There are a number of possible interpretations:

(i) The low-energy group represents vibrations of H in octahedral sites.

(ii) The vibrations are due to hydrogen in U-shaped potential wells in a minority phase, as it is found for $ZrNiH_x$ [21].

(iii) They are vibrations of hydrogen in sub-surface states, similar to those found for palladium hydride [22].

(iv) The low-energy group is due to bending- and stretching-vibrations of OH-groups bound to near-surface metal atoms.

The first three explanations sound unlikely for the following reasons. (i): Octahedral sites, which can be occupied by H are hard to explain with respect to the $P6_3/mmc$-symmetry of C14 Laves phases. Only tetrahedral sites should be occupied. (ii): Regarding the off-stoichiometry of $TiMn_{1.5}$ a minority phase may certainly be present, but with totally different hydrogen potentials. (iii): For the given structure, this explanation would demand very anomalously enlarged lattice parameters in the sub-surface region.

The most convincing explanation is (iv), since it is known from Auger electron spectroscopic work [10, 18, 23] that due to hydrogen interaction with $AB_{1.5}$- and AB_2-compounds (A = Ti, Zr; B = Mn) a chemically induced segregation of Ti(Zr) and bulk oxygen impurities simultaneously takes place. Thus, the formation of Ti–OH bonds (Zr–OH bonds) at the surface of the compound seems quite obvious. In fact it is possible to decide between the explanations (i)–(iii) on the one hand and the explanation (iv) on the other, if the results of the separation factor measurements are included into the interpretation. We therefore refer to the stretching and bending vibrations of finely divided $Ni(OH)_2$ as measured by IINS [24]. The values are given in table 4, together with the well-known O–H valence vibration.

Table 4 shows that the low-energy peak group (peaks 1, 2 and 3) may certainly reflect vibrations of type A, B and possibly D. For the case of Ti–OH species (case (iv)), the isotope separation factor at low hydrogen concentrations would be determined by the vibrations ν(O–H) at 400 meV and δ(O–H) at 111.5 meV.

In cases (i)–(iii), on the other hand, hydrogen vibrates in interstitial positions with flat potential wells and hence the isotope separation factor at low H-contents would be governed by the vibrations of the low-energy peak group (peaks 1, 2 and 3).

A straightforward calculation of the separation factor based on the localised harmonic oscillator model [6] and the two sets of vibrations will, therefore, enable a decision between explanations (i)–(iii) and explanation (iv).

The isotope exchange reaction between the gas-phase and the solid phase with hydrogen in the two different types of site (e.g. surface- and bulk states) will equilibrate at a point, which is governed by an averaged equilibrium separation factor.

$$\bar{\alpha} = \alpha_{Lo}\Gamma_{Lo} + \alpha_{Hi}\Gamma_{Hi} \tag{2}$$

Γ_{Lo} and Γ_{Hi} are the surface and bulk fractions of H as given in table 2 and α_{Lo} and α_{Hi} are the individual equilibrium separation factors for the distribution of hydrogen between gas phase and the type of site in question. For hydrogen in interstitial sites of (nearly) cubic symmetry α can be calculated from the equation

$$\alpha = \left[\frac{\sinh(u_T)}{\sinh(u_H)}\right]^3 \left[\frac{Z_{HT}}{Z_{HH}}\right]^* \tag{3}$$

as was shown elsewhere [6].

In this expression u_T and u_H are determined by the localised vibrations of the tracer isotope, tritium (T), and of the excess isotope, protium (H), i.e. $u_i = h\nu_i/2kT$. The term $(Z_{HT}/Z_{HH})^*$ means the ratio of the partition functions of the gas-phase molecules indicated (without symmetry numbers). This quantity is accessible from literature data [25].

For hydrogen bound in OH-groups, the separation factor is determined by the stretching and bending vibrations of hydrogen:

$$\alpha = \frac{\sinh(u_{T,\upsilon})}{\sinh(u_{H,\upsilon})}\left[\frac{\sinh(u_{T,\delta})}{\sinh(u_{H,\delta})}\right]^2 \left[\frac{Z_{HT}}{Z_{HH}}\right]^* \tag{4}$$

Hence, if we assume hydrogen to be in near-surface interstitial positions of type (i)–(iii), equation (3) holds, with $\upsilon_H = 74$ meV, the dominant peak of the low-energy group. Using the harmonic approximation ($\upsilon_H = \upsilon_T\sqrt{3}$) yields $\alpha_{Lo} = 3.0$ at 273 K.

If, otherwise, H is bound via O to the metal, case (iv), equation (4) should be used and the frequencies of the stretching and bending vibrations as given by C and D in table 4 operate on the separations factor. Now, using the harmonic approximation, it turns out that $\alpha_{Lo} = 0.109$ at 273 K.

For diminishing hydrogen content in high-energy states ($\Gamma_{Hi} = 0$) the separation factor should approach the value 3 in cases (i)–(iii) but the value 0.1 in case of (iv). From table 3 there is clear evidence that the latter is true. We may thus conclude that activated $Ti_{0.4}Mn_{0.6}$ contains $Ti(OH)_x$-species in near-surface regions.

Figure 5 shows plots of the measured separation factor α versus n (circles). The dashed vertical lines indicate the two-phase region and it is seen that there is a small step from $\alpha = 0.75$ to $\alpha = 0.82$ due to the softening of the localised hydrogen modes on crossing this region (lattice expansion).

Figure 5 also contains calculated values of α from equation (2), taking Γ_{Lo} and Γ_{Hi} from table 2. α_{Lo} was calculated either by equation (3) with υ_H as given by peak 1 in table 1 (triangles) or by equation (4) with the vibrations C and D given in table 4 (squares). In both cases the value α_{Hi} was estimated by approaching the complicated peak-structure of the high-energy group (superposition of C_{3v} and C_{2v} symmetry) by a doublet according to D_{2h}-symmetry [6]. For this purpose the dominant peak 5 in table 1 was associated with the two-fold degenerated vibration of the D_{2h}-doublet. This procedure may be vindicated

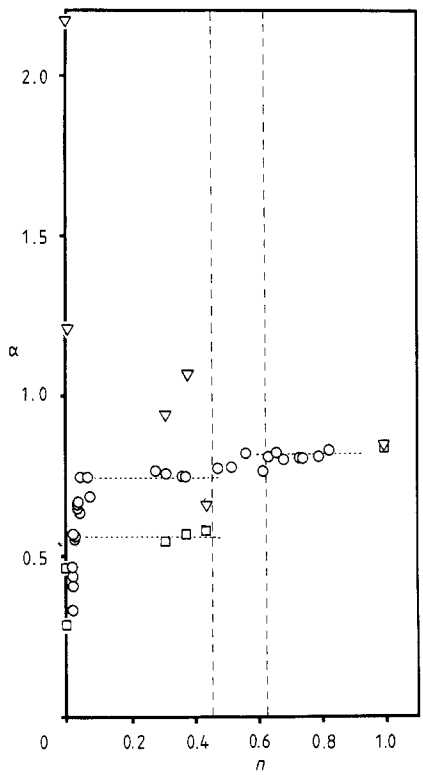

Figure 5. Plot of the measured equilibrium separation factors versus n (circles). Calculated values based on the IINS-results are indicated by triangles (assuming precursor H vibrating in spacious bulk interstitial sites) and by squares (assuming precursor H bound via O to the metal-surface). For details see text.

by the good agreement between measured and calculated values of α at high H-concentrations ($\Gamma_{Hi} = 1$).

The squares follow the measured α-values in a satisfactory manner, especially at low and high H-contents. The deviations at medium H-concentrations are mainly due to the already mentioned simplifications as neglecting the complicated site geometry of occupied bulk states and possibly hydride precipitations, which cause lattice distortions.

The triangles, however, are in contradiction to the measured values of α versus n and this behaviour is most pronounced at low hydrogen contents in the precursor region (see figure 1). Thus, the separation factor results imply that any type of interstitial sites in the bulk may be eliminated as a possible origin of the precursor region and hence also as the origin of the group of low-energy peaks. We must therefore conclude that surface species of the type $Ti(OH)_x$ are responsible for both the dominant peak of the low-energy group in the IINS-spectra and the enhanced hydrogen solubility in the precursor region of the sorption isotherms.

6. Conclusions

We have demonstrated the usefulness of a combination of IINS (incoherent inelastic neutron scattering) and isotope separation factor measurements in determining the hydrogen site occupation in a hydrogen storage material. In particular we have been able to identify the 'precursor' sites (i.e. the small population of highly stable sites) in the $Ti_{0.4}Mn_{0.6}H_n$ system as being caused by –OH groups formed on the surface of the

activated material because although we observe a peak at about 75 meV—due to oxygen vibrations—the isotope effect is determined by the much higher frequency O–H (T) vibration. It is likely that precursors in other finely divided intermetallic hydride systems will have a similar origin.

Acknowledgments

The authors would like to thank the following for helpful discussions and technical advice: M J Benham (Birmingham), A Kollmar (ILL), R Sinclair, C Windsor and D Cummins (Harwell Laboratory). They would also like to record their gratitude to the SERC and ILL for the provision of neutron beam time.

References

[1] Springer T 1979 *Z. Phys. Chem. NF* **115** 141
[2] Richter D 1983 *J. Less-Common Met.* **89** 293
[3] Hunt D G and Ross D K 1976 *J. Less-Common Met.* **49** 169
[4] Ross D K, Martin P F, Oates W A and Khoda-Baksh R 1979 *Z. Phys. Chem. NF* **114** 221
[5] Hempelmann R, Richter D and Stritzker B 1982 *J. Phys. F: Met. Phys.* **12** 79
[6] Sicking G and Andreev B 1987 *Ber. Bunsenges. Phys. Chem.* **91** 177
[7] Gamo T, Moriwaki Y, Yamashita T and Fukuda M 1976 *Synopses 1976 Autumn Meeting of the Japan Institute of Metals, Sendai* p 307
[8] Gamo T, Moriwaki Y, Yanagihara N and Iwaki I 1983 *J. Less-Common Met.* **89** 373
[9] Sicking G, Magomedbekov E and Hempelmann R 1981 *Ber. Bunsenges. Phys. Chem.* **85** 686
[10] Sicking G, Albers P and Magomedbekov E 1983 *J. Less-Common Met.* **89** 373
[11] Yamashita T, Gamo T, Moriwaki Y and Fukuda M 1977 *Nippon Kinzoku Gakkaishi* **41** 148
[12] Suda S, Kobayashi N and Yoshida K 1980 *J. Less-Common Met.* **73** 119
[13] Albers P W, Sicking G H, Earwaker L G and England J B A 1987 *Ber. Bunsenges. Phys. Chem.* **91** 573
[14] Albers P, Sicking G and Harris I R 1988 *Z. Metallkde.* **79** 24
[15] Didisheim J J, Yvon K, Shaltiel D and Fischer P 1979 *Solid State Commun.* **31** 47
[16] Fruchart D, Soubeyroux J L and Hempelmann R 1984 *J. Less-Common Met.* **99** 307
[17] Froitzheim H, Ibach H and Lehwald S 1976 *Phys. Rev. Lett.* **36** 1549
[18] Sicking G and Magomedbekov E 1982 ed. T N Veziroglu *Proc. Int. Symp. on Metal–Hydrogen Systems, Miami Beach, FL, April 13–15, 1981* (Oxford: Pergamon)
[19] Rahman A, Sköld K, Pelizzari C, Sinha S K and Flotow H E 1976 *Phys. Rev.* B **14** 3630
[20] Hempelmann R, Wicke E, Hilscher G and Wiesinger G 1983 *Ber. Bunsenges. Phys. Chem.* **87** 48
[21] Benham M J, Browne J D and Ross D K 1984 *J. Less-Common Met.* **103** 71
[22] Nicol J M, Rush J J and Kelley R D 1987 *Phys. Rev.* B **36** 9315
[23] Jungblut B and Sicking G 1989 *Z. Phys. Chem., NF* at press
[24] Renouprez A J, Fouilloux B and Candy J P 1979 *Surf. Sci.* **83** 285
[25] Bron J, Chang Chen Fee and Wolfsberg M 1973 *Z. Naturf.* a **28** 129